FRONT DYNAMICS IN A LIQUID CRYSTAL LIGHT VALVE WITH FEEDBACK

M.G. CLERC, A. PETROSSIAN, S. RESIDORI, AND C.S. RIERA

Abstract. The Fréedericksz transition can become subcritical in the presence of a feedback mechanism that leads to the dependence of the applied electric field onto the liquid crystal re-orientation angle. We have given evidence of a first-order Fréedericksz transition in a Liquid Crystal Light Valve with optical feedback. We have characterized this transition both experimentally and theoretically, with the determination of the bistability region as well as of the transition and the Maxwell points. In one and two spatial dimension, we have investigated the propagation of the fronts connecting the stationary states. In particular, in one spatial dimension we have measured the velocity of front propagation. Theoretically we have used a minimal description, subcritical Landau equation, valid close to the Fréedericksz transition. This description is in a good agreement with the experimental observations.

1. Introduction

Liquid crystals under the influence of electric and magnetic fields exhibit a large variety of complex dynamical behaviors, like electro-convection [1], optical instabilities [2] and spiral patterns [3, 4]. Pattern formation, defect dynamics and spatio-temporal instabilities [5, 6].

One of the most well-studied phenomena in the physics of liquid crystals is the field-induced distortion of a homeotropic or planar aligned liquid-crystal film, called the Fréedericksz transition [7]. This transition is usually a second order one [8, 9]. Recently, we have shown that the Fréedericksz transition in Liquid Crystal Light Valve (LCLV) with feedback can become to first order one [10]. The purpose of this article is to shown that the experimental observations in LCLV with feedback close to Fréedericksz transition. Experimentally, we observe a hysteresis region of the first-order Fréedericksz transition. In the bistable region, we study the propagation of the fronts connecting the stationary states. We have performed experiments either in one or two spatial dimensions, and we have measured the velocity of the fronts.

1.1. Experimental setup.

Experimental setup. A LCLV consists essentially in a nematic liquid-crystal film sandwiched between a glass and a photoconductive plate over which a dielectric mirror is deposed. Coating of the two bounding plates induces a planar anchoring (nematic director $\vec{n}$ parallel to the walls) of the liquid crystal film. Moreover, transparent electrodes covering the two plates permit the application of an electric field across the liquid-crystal layer. The photoconductor behaves like a variable resistor, which resistance decreases for increasing illumination.

The light-driven feedback in LCLV is obtained by sending back onto the photoconductor the light which has passed through the liquid-crystal layer and has been reflected by the dielectric mirror. This is realized by means of an optical fibre bundle. The voltage V_0 applied to the LCLV is sinusoidal and of frequency $f = 20$ KHz, which is much larger than the liquid crystal response time.

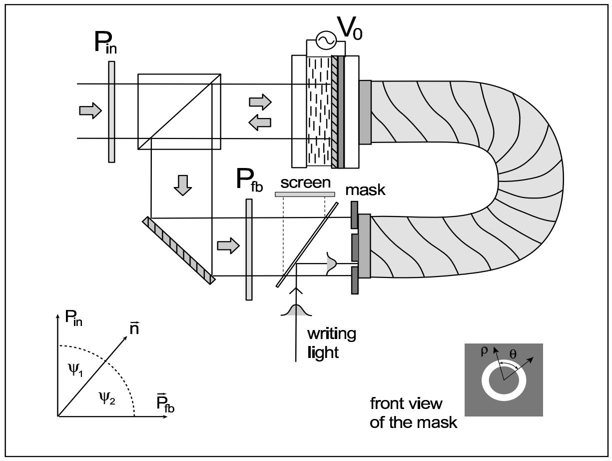

FIGURE 1. Experimental setup. Two confocal lenses, not displayed in the scheme, provide a 1 : 1 image-forming system from the front side of the LCLV to its rear side. The optical feedback loop is closed by a fibre bundle, which is aligned in order to avoid any rotation or shift. P_{in} and P_{fb} are, respectively, the input and feedback polarizer. Their orientation with respect to the liquid crystal director $\vec{n}$ is indicated in the left bottom of the figure. In the right bottom it is shown the mask used for the 1D experiments.

The experimental setup, as shown in Fig.1, is designed in such a way that the light beam experiences no diffraction as well as no geometrical transformation, so that no transverse structures are induced close to the Fréedericksz transition. The light intensity I_w reaching the photoconductor is given by [5]

$$I_w = |\cos(\psi_1)\cos\psi_2 + \sin\psi_1 \sin\psi_2 e^{-i\beta cos^2\theta})|^2 I_{in} \tag{1.1}$$

where θ is the liquid crystal re-orientation angle, $\beta \equiv 2kd\Delta n cos^2\theta$ is the overall phase shift experienced by the light travelling forth and back through the liquid crystal layer, I_{in} is the input intensity, ψ_1 and ψ_2 are the angles formed by the input and feedback light polarization with the liquid crystal director $\vec{n}$, respectively, $k = 2\pi/\lambda$ is the optical wave number, d is the thickness of the liquid crystal layer and Δn is the difference between the extraordinary ($\|$ to $\vec{n}$) and ordinary ($\perp$ to $\vec{n}$) index of refraction of the liquid crystal. In our experiment, $\beta \simeq 120$ since $\lambda = 633$ nm, $\Delta n = 0.2$, $d = 30$ μm. Input light intensity is typically around $I_{in} \simeq 0.9$ mW/cm^2.

2. Minimal description

The dynamical evolution of the nematic film is characterized by the Frank free energy. We express this free energy by taking into account the feedback effect as well as the usual non linear elastic term. Then, close to the transition point,

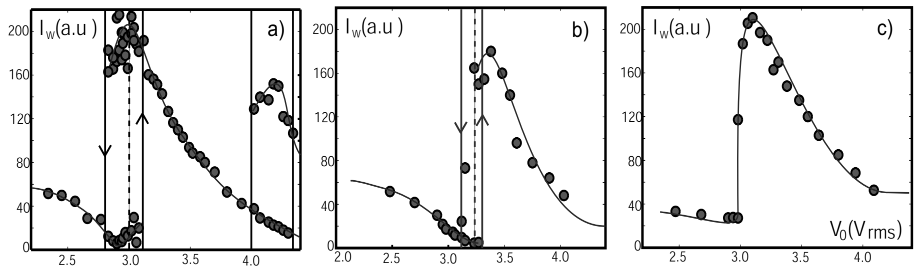

FIGURE 2. Experimental bifurcation diagrams recorded for three different values of the polarizer angle: a) $\psi_1 = \psi_2 = 45^o$, b) $\psi_1 = 45^o$ and $\psi_2 = 38^o$, c) $\psi_1 = 45^o$ and $\psi_2 = 18^o$. Arrows mark the limits of the hysteresis region, dashed lines indicate the Maxwell point and thin lines are guides for the eyes. In c) the bifurcation has become a second-order one.

we can derive an amplitude equation for the first excited spatial mode. Let us call $u(x, y; t)$ the order parameter that describes the amplitude of first excited spatial mode ($\{x, y\}$ are the coordinates that describe transversely the nematic liquid crystal sample). Since, under the influence of an horizontal electric field, the molecules can turn indifferently clockwise or counterclockwise, the order parameter is invariant under reflection transformation, so that $u(x, y; t) \to -u(x, y; t)$. The order parameter satisfies the equation [10]

$$\partial_t u = c_1 u + c_3 u^3 + c_5 u^5 + \frac{K}{\gamma}\nabla_\perp^2 u. \tag{2.1}$$

where

$$\begin{aligned}
c_1 &= \gamma^{-1}(-\frac{K\pi^2}{d^2} + \epsilon_a E_0^2 + A\epsilon_a(A + 2E_0) + 2B(A + E_0)(\epsilon_a \cos\beta + \beta\epsilon_\perp \sin\beta) \\
&\quad + B^2(\frac{\epsilon_a}{2}(1 + \cos 2\beta) + \beta\epsilon_\perp \sin 2\beta)), \\
c_3 &= \gamma^{-1}(\frac{1}{3}\frac{K\pi^2}{d^2} - \frac{2}{3}\epsilon_a E_0^2 - B(E_0 + A)((\frac{4}{3}\epsilon_a + \frac{8}{\pi^2}\beta^2\epsilon_\perp)\cos\beta \\
&\quad - \frac{2}{3}A\epsilon_a(A + 2E_0) - ((\frac{8}{\pi^2} + 1)\epsilon_a - \epsilon_\perp)\beta\sin\beta) - B^2(\frac{\epsilon_a}{3} + (\frac{8}{\pi^2}\beta^2\epsilon_\perp \\
&\quad + \frac{\epsilon_a}{3})\cos 2\beta + (\frac{\epsilon_\perp}{2} - \frac{\epsilon_a}{2}(\frac{8}{\pi^2} + 1))\beta\sin 2\beta)), \\
c_5 &= \gamma^{-1}(\frac{2}{15}\frac{K\pi^2}{d^2} - \frac{4}{\pi^2}(B(A + E_0)(((\frac{4}{\pi^2} + 1)\epsilon_a - \epsilon_\perp)\beta^2\cos\beta \\
&\quad + (\frac{64 + 9\pi^2}{48}\epsilon_a + \frac{4\beta^2}{\pi^2}\epsilon_\perp)\beta\sin\beta) - B^2(((\frac{4}{\pi^2} + 1)\epsilon_a - \epsilon_\perp)\beta^2\cos 2\beta \\
&\quad + (\frac{64 + 9\pi^2}{48}\epsilon_a + \frac{4\beta^2}{\pi^2}\epsilon_\perp)\beta\sin\beta\cos\beta)),
\end{aligned}$$

$$\begin{aligned}
A &\equiv \frac{1}{4}[\cos 2(\psi_1 - \psi_2) + \cos 2(\psi_1 + \psi_2) + 2]\alpha I_{in}, \\
B &\equiv \frac{1}{4}[\cos 2(\psi_1 - \psi_2) - \cos 2(\psi_1 + \psi_2)]\alpha I_{in},
\end{aligned}$$

γ and k are the rotational viscosity and elastic constant of the nematic film, respectively, and $E_0 = V_0/d$. The coefficient c_1 is proportional to the bifurcation parameter. The non-linear coefficients c_3 and c_5 characterize the nature of the bifurcation.

For negative and order one c_3, one can neglect asymptotically the coefficient c_5. Then, the Fréedericksz transition is a second order type, as is illustrated in Fig.2c. As long as c_3 is small, the system is asymptotically described by the above model. For positive c_3 and negative c_5 the Fréedericksz transition becomes first-order type, as shown in Fig.2(a)(b). It is important to note that the voltage V_o applied to the nematic film is the control parameter whereas the polarizer angles control the nature of the bifurcation, which can be changed from first to second order type.

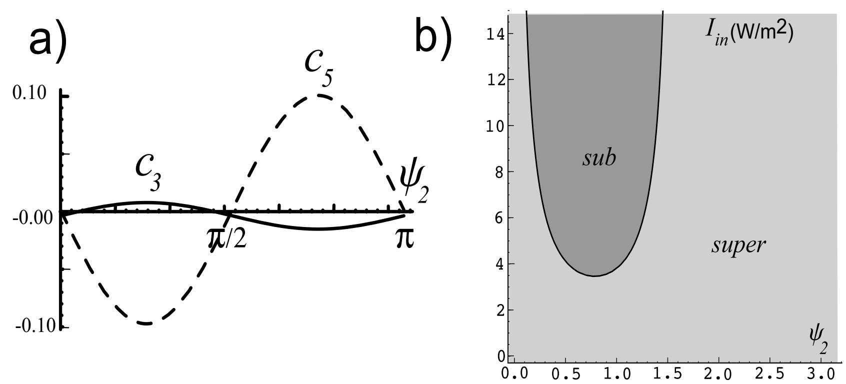

FIGURE 3. a) Coefficients c_3 and c_5 as a function of the polarizer angle ψ_2, $c_1 = 0$ and $\psi_1 = \frac{\pi}{4}$. b) Phase diagram as a function of the input intensity I_{in} and polarizer angle ψ_2 (radian). Solid line corresponds to $c_3 = 0$, marking the border between the subcritical and the supercritical case.

In Fig.3 we show the behavior of the coefficients c_3 and c_5 as a function of the feeedback polarizer angle ψ_2 .

Henceforth, we will limit ourselves to the case $0 < c_3 \ll 1$ and $c_5 > 0$. By scaling the time, the space coordinates and the amplitude of the order parameter, the above model equation, Eq.(2.1), takes the form

$$\partial_t u = \mu u + u^3 - u^5 + \nabla_\perp^2 u \tag{2.2}$$

where $U_o = (c_3/c_5)^{1/2}$, $T_o = c_5/c_3^2$, $R_o = K\left(c_5/c_3^2\right)$ and $\mu = c_1 c_5/c_3^2$. Hence, the first-order Fréedericksz transition is fully characterized by a single parameter μ, which is proportional to the bifurcation parameter c_1.

2.1. **stationary states.** The main feature of a first order transition is the appearance of hysteresis in the bifurcation diagram [12], that is, the system exhibits bistability for a certain parameter range. In Fig.4 it is shown the bifurcation diagram associated to the above model equation, Eq.(2.2). For negative μ and large enough amplitude ($\mu < -0.25$), the system has only one stable state $u(x,t) = u_0 = 0$. This state corresponds to a planar unperturbed alignment of the liquid crystal film. When the bifurcation parameter is increased, this steady state becomes unstable for positive μ. This transition is a subcritical pitchfork bifurcation and in our experiment it corresponds to a first-order Fréedericksz transition. As a result, for $1/4 \leq \mu \leq 0$, the model exhibits bistability and the stationary solutions are given by

$$
\begin{aligned}
u_o &= 0,\\
u_{+,\pm} &= \pm\frac{\sqrt{1+\sqrt{1+4\mu}}}{2},\\
u_{-,\pm} &= \pm\frac{\sqrt{1-\sqrt{1+4\mu}}}{2}.
\end{aligned}
$$

The states u_o and $u_{+,\pm}$ are stable and whereas $u_{-,\pm}$ are unstable. Note that Eq.(2.2) is a variational one and is characterized by the potential

$$V\left(u\right) = -\mu\frac{u^2}{2} - \frac{u^4}{4} + \frac{u^6}{6}.$$

It is now straightforward to derive the Maxwell point, which is located at $\mu = \mu_M = -3/16$, for which the system satisfies $V\left(u_o; \mu = \mu_M\right) = V\left(u_{+,\pm}; \mu = \mu_M\right)$.

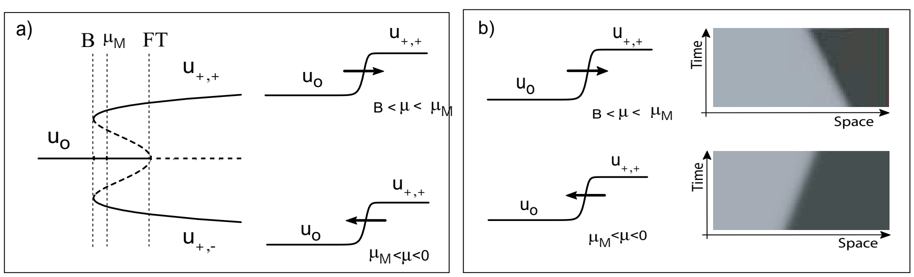

FIGURE 4. The generic features of a subcritical bifurcation diagram and the associated directions of the front propagation. a) B, μ_M and Fréedericksz transition mark the beginning of the hysteresis region, the Maxwell point and the Fréedericksz transition point, respectively. The front connecting the u_0 to the $u_{+,+}$ state propagates towards the most stable state, this one being u_0 or $u_{+,+}$ depending on the value of the bifurcation parameter μ with respect to the Maxwell point μ_M. The front dynamics are the same on the lower branch $u_{+,-}$. b) The front propagation is shown together with its corresponding spatio-temporal diagram, on both the contracting and the expanding side of the bifurcation diagram.

2.2. **Experimental measurement of the bifurcation diagram.** We measure the intensity I_w reaching the photoconductor as function of the voltage V_0 applied to the nematic film. A typical bifurcation diagram, recorded for $\psi_1 = \psi_2 = 45^o$, is shown in Fig.5. Note that the Fréedericksz transition takes place at $V_0 \simeq 3.2$ V r.m.s. Moreover the transition from the non-oriented state to the oriented one is characterized by a large hysteresis region, that we can clearly identify when the applied voltage V_0 is decreased. In the bistability region, we can trigger the transition to the upper state by sending into the feedback loop an additional writing light (low power *He-Ne* laser) which acts as a small perturbation. It is important to remark that our experimental procedure does not allow to distinguish between the two possible rotations of the molecules (θ and $-\theta$). Indeed, we measure I_w, which is related to $\cos^2(\theta)$. A quantity sensitive to the sign of θ would instead lead to a bifurcation diagram with two symmetric branches, as the one shown in Fig.4. However, in any physical device there is always a small symmetry breaking which induce a preferential selection of one of the two possible states, rendering the bifurcation an imperfect one. It is indeed the case for the LCLV, since for stability reasons an extremely low pre-tilt is imposed on the surface at the fabrication stage. For this reason, we have to consider only one half of the ideal bifurcation diagram and our experimental procedure fully describes the system behavior.

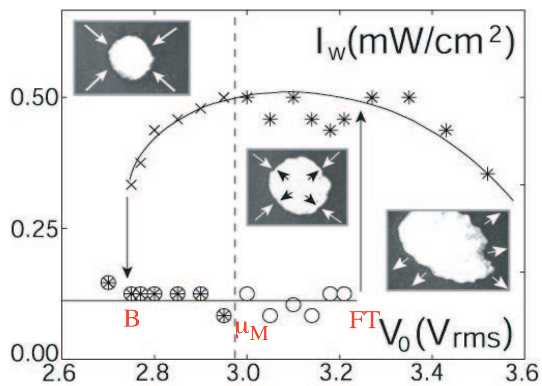

FIGURE 5. Experimental bifurcation diagram and front propagation: open circles are dark states with writing light off; stars are white states with writing light off; cross are white states with writing light on. The white state shrinks to zero or expands to infinity depending on the initial location of the perturbation. Beyond (and close to) the Maxwell point it exists a critical droplet radius for which the front velocity is zero.

3. Front propagation

In the precedent description, we have considered only homogeneous stationary states, but in fact a perturbation of these states gives rise transients characterized by a rich front dynamics. At the onset of bistability ($-0.25 < \mu \leq \mu_M$), a spatially localized perturbation of the metastable state leads locally to the appearance of the other stable state. Thus, the system displays a moving interface that connects two steady states, so called a *front* . The front moves into the less energetically favorable state with a well defined velocity, as is represented in the spatio-temporal diagram in Fig.4. In the case of one or two spatial dimension and small interface curvature, the front velocity is proportional to the energy difference between the two stables states.

In two dimensions, the velocity of the front can be modified by its curvature, the so called Gibbs-Thomson effect or non variational dynamics [13]. Increasing the bifurcation parameter, at some point the metastable state becomes energetically equivalent to the other one, thus the front stops to propagate. By further increase of the bifurcation parameter, the front velocity is reversed. A generic bifurcation diagram with reflection symmetry, together with the associated directions of the front propagation, is shown in Fig.4.

Once determined the three critical points of the model Eq. (2.2) and of the experiments, that is, beginning of the bistability B $\mu = -1/4$, Maxwell point $\mu_M = -3/16$ and Fréedericksz transition transition point $\mu = 0$, the front dynamics is entirely characterized. For $1/4 \leq \mu \leq 0$, the system displays several fronts between the stationary states (u_o, $u_{+,\pm}$, $u_{+,\mp}$, and $u_{-,\mp}$):

- $1/4 < \mu < \mu_M$, the fronts $\{u_o; u_{+,\pm}\}$ propagate towards $u_{+,\pm}$, respectively, see. Fig.4. Correspondingly, if one perturbs enough the planar state then the system relaxes quickly to different domains between the stable states, and later on the less favorable domains disappear.
- $\mu = \mu_M$: the fronts $\{u_o; u_{+,\pm}\}$ or kink solutions do not propagate, because both states are energetically equivalent. In one spatial dimension, when the system exhibits several domains, constituted by the alternation of kink and anti-kink solutions, these domains disappear slowly, because of the attractive exponential interaction between kink and anti-kink [14]. In two spatial dimensions, the curvature effect leads to a faster dynamics of domains.
- $\mu_M \leq \mu \leq 0$: the model predicts fronts $\{u_o; u_{+,\pm}\}$ that propagate towards the planar state u_o, which is now metastable. In this parameter region, the system also presents the *kink or wall* solution between the symmetrical states $u_{+,+}$ and $u_{+,-}$. It is important to note that these fronts are the analog of Ising walls in magnetic films. In one dimension, the domains are transient states, whose mean life time is quite large, that is, they are metastable states. By decreasing the bifurcation parameter below the Maxwell point ($\mu < \mu_M$), the wall solution becomes unstable. Indeed, the core of the front pass through the planar state ($u_0 = 0$), so that it starts to nucleate the u_0 state which is energetically more favorable [15]. Experimentally, this kind of wall is not observed in the LCLV, because the liquid crystal film has a small pre-tilt due to the anchoring conditions.
- For $\mu > 0$: the state becomes unstable through a pitchfork bifurcation. Fluctuations of the initial state give rise to the appearance of the other states. In this case there is a front connecting a stable state with an unstable one ($\{u_o; u_{+,\pm}\}$). This type of front is called Fisher-Kolmogorov-Petrosvky-Piskunov (FKPP) [16, 17]. At variance with the normal front, the velocity of the FKPP front is not determined by the difference of energy between the two connected states. Instead of a given velocity, there is an infinity of different possible velocities, each one determined by the initial conditions. This set of possible velocities is lower bounded by a minimum value v_{min} [18, 19]. At longer time, the dynamics is characterized by coarsening $u_{+,+}$ and $u_{+,-}$of the $u_{+,+}$ and $u_{+,-}$ domains. This coarsening is an effect driven by the influence of the front curvature on its own velocity.

3.1. **1D experiments: measurement of the front velocity.** We have measured the velocity of the normal fronts connecting the stable states that are present in the subcritical regime. In order to avoid the influence of curvature effects on the front velocity, we have realized 1D experiments by inserting a ring mask in the feedback loop (see Fig.1). In these conditions, we set the values of the voltage V_0

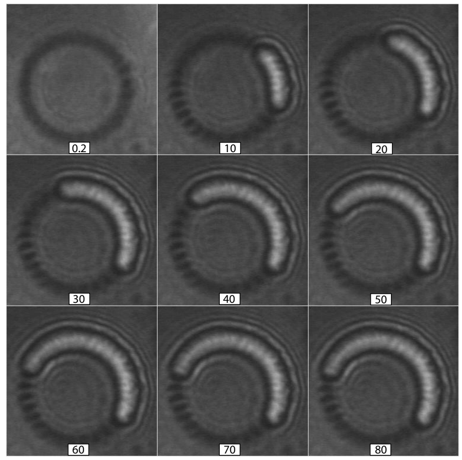

FIGURE 6. Snapshots of the front propagation along the ring, recorded at $V_0 = 3.20\ V_{rms}$. White rectangles contain the indication of the instantaneous time (in seconds) of the image acquisition.

applied to the LCLV close to the Fréedericksz transition point. Then, by means of a computer controlled synthesizer, we switch on and off V_0 and we record the images of the front apparition and of its propagation along the ring. Instantaneous snapshot recorded for $V_0 = 3.20\ V_{rms}$ are shown in Fig. 6.

Above the Maxwell point, the front arise naturally by nucleation over some inhomogeneity that is present in the LCLV. The nucleation point is not fixed but changes by small adjustments of the ring mask or very small misalignment of the feedback light. Indeed, the nucleation point is just the point that is the more favored by any symmetry breaking mechanism. Below the Maxwell point, we need to switch on the writing light in order to develop the white state and to induce a front in the ring. When we switch off the writing light, the front velocity is reversed and the white state contracts to zero.

Either below or above the Maxwell point, we have measured the front velocity by the following procedure. Once recorded a time sequence of images, we have chosen a circle passing through the median radius of the ring and then, for each image, we have unfolded this circle over a line. This way, we have constructed the spatio-temporal diagram of each recorded set of images. The spatio-temporal diagram recorded at $V_0 = 3.20\ V_{rms}$ and corresponding to the snapshots displayed in Fig.6, is shown in Fig.7. The front velocity can be evaluated by simply measuring the ratio between the horizontal (space-x) and vertical (time-t) displacements.

The resulting front velocities are shown in Fig.8 as a function of the applied voltage V_0. On this Figure, we can identify the Maxwell point where the front velocity goes to zero and the Fréedericksz transition point, beyond which the fronts become of a FKPP type. The regime of FKPP fronts is characterized by a transient propagation with a quite high velocity, which then relaxes to the minimal one. In Fig.8 we report both the transient and the steady-state velocity for the FKPP fronts. In Fig.9 we show a spatio- temporal diagram for a FKPP front, recorded at $V_0 = 3.50\ V_{rms}$ .We can see the presence of two different slopes, that characterize

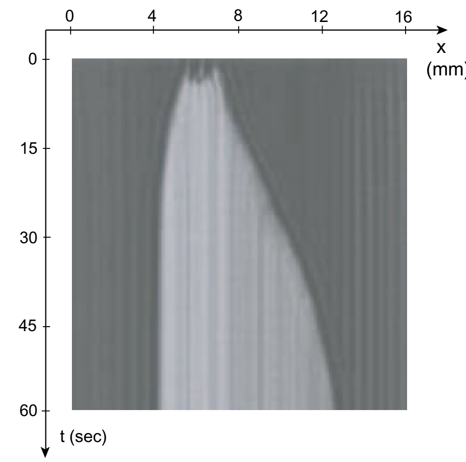

FIGURE 7. Spatiotemporal diagram showing the propagation of the front at $V_0 = 3.20\ V_{rms}$, corresponding to the images in Fig.6. The front velocity is $v_f = 0.2\ mm/s$.

the transient and the steady-state propagation, respectively. Numerical simulation of the Model (2.2) exhibit the same behavior as is illustrated in Fig.9.

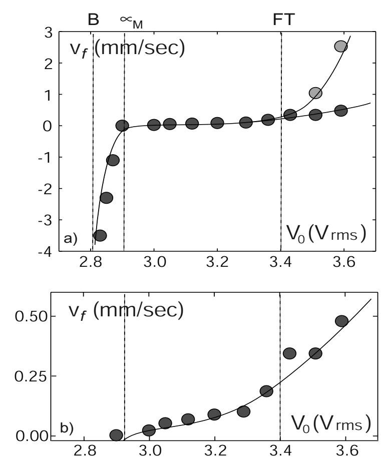

FIGURE 8. Front velocity as a function of the bifurcation parameter V_0. Dashed lines mark the three critical points: B, μ_M, FT. Lighter circles in a) represent the transient velocities of the FKPP fronts. In b) we show en enlargement of the central region.

4. 2D SPATIAL DYNAMICS: EXPERIMENTAL RESULTS AND COMPARISON WITH THE MODEL

In Fig.5, we show I_w as a function of V_0 and in the presence of feedback. The transition point is characterized by an abrupt change in the intensity, which reaches its maximum value. Notice that I_w is measured by a small area photodiode, i.e., it is a local measurement taken at the center of the feedback beam. By looking at the entire image of the feedback beam with a CCD camera, we see that the transition point is characterized by a white spot developing over a dark background. In the course of time, the front of the white spot expands and the white state overcomes the dark one. For the model, this represents the FKPP front between the unstable state $u_0 = 0$ and the stable state $u_{+,\pm}$. By further increasing the voltage, the LCLV birefringence changes and the white state becomes *grey* until the dark value is reached again. Successive transitions to the white state are present for larger values of the applied voltage. These states correspond to parameter values far from the Fréedericksz transition and have already been investigated in optical pattern formation [20].

By decreasing the voltage, we observe a hysteresis cycle. In order to determine the size of the bistable region, we inject an additional light spot (low power He-Ne laser) into the feedback loop. This acts as a small perturbation, triggering the transition from the dark state to the white one. The white state persists when we block the additional writing light, while it switches to the dark state if we perturb the feedback. In Fig.5, the arrows delimit the region over which this writing-erasing procedure is robust. Notice that spatial inhomogeneities and other noise sources can influence the stability of the two states.

In Fig.5 are illustrated the three representative images of front dynamic in 2D. These images show the direction of the front propagation, depending on the mutual stability of the white and the dark homogeneous state. The dashed line marks the point at which the front propagation is zero, usually called the *Maxwell point*. Below this point the white state is less stable than the dark one and the white spot, once created by the writing light, contracts to zero. Above the Fréedericksz transition point, the white spot nucleates spontaneously and its front expands until the white state covers all the background. In between, the front of the spot expands or retracts depending on the size of the perturbation.

Note that the Maxwell and the Fréedericksz transition points are slightly shifted with respect to the 1D case. This is indeed related to the front curvature effect, which affects the front velocity in 2D. As a consequence, in the 2D experiments the location of the Maxwell point is overestimated whereas the Fréedericksz transition point is shifted to smaller values of the bifurcation parameter.

5. Conclusions

The Fréedericksz transition can become subcritical in the presence of a feedback mechanism that leads to the dependence of the applied electric field onto the liquid crystal re-orientation angle. We have performed 2D and 1D experiments in a LCLV with optical feedback and reported the features of a first-order transition over a spatially extended system. Thus, we have opened the possibility to investigate the spatial dynamics related to front propagation.

In order to account for the rich dynamics observed in the experiment, we have used a Landau normal form as a standard model for a subcritical bifurcation. Then, we have been able to express the coefficients as a function of all the relevant physical parameter of the experiment. This allow us a quantitative comparison between the predictions of the model and the experimental findings.

We have depicted the qualitative dynamics of front propagation in one and two spatial dimension. In the 1D cases, the theoretical model provides all the main

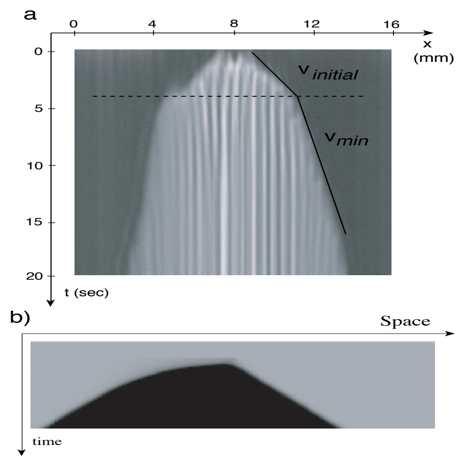

FIGURE 9. a) Experimental spatiotemporal diagram recorded at $V_0 = 3.50\ V_{rms}$, showing the propagation of a FKPP front. b) Numerical spatiotemporal diagram of a FKPP front.

features of the dynamics of normal and FKPP front. Experimentally, we have observed these fronts and measured their velocity in one dimension. We have also determined the Maxwell point, where the front velocity is zero, and the Fréedericksz transition point, beyond which the front becomes of a FKPP type.

In conclusion, we have presented here quite a complete description of the spatial features related to the first order Fréedericksz transition, giving a general model which is supported by a considerable amounts of experimental observations. Moreover, our experimental approach opens the way to further investigations in view of the observation of other fundamental phenomena in the spatial dynamics of fronts.

Acknowledgement 1. *We would like to thank T. Nagaya for technical advices and fruitful discussions. Simulation software developed at INLN has been used for study the normal form (2.2). This work has been supported by the ACI Jeunes of the French Ministry of Research (2218 CDR2). M.G.C. thanks the support of Programa de inserción de científicos Chilenos of Fundación Andes, FONDAP grant 11980002 and FONDECYT projects 1020782. A.P. acknowledges support from CNRS.*

References

[1] See, .e.g., L. Kramer and W. Pesch in *Pattern Formation in Liquid Crystals*, edited by A. Buka and L. Kramer (Springer-Verlag, New york, 1996).
[2] N.V. Tabiryan, A.V. Sukhov and B. Ya. Zel'dovich, Mol. Cryst. Liq. Cryst. **136**, 1 (1985).
[3] T. Frisch, S. Rica, P. Coullet and J.M. Gilli, Phys. Rev. Lett. **72,** 1471 (1994).
[4] T. Borzsonyi, A. Buka, A.P. Krekhov, O.A. Scaldin and L. Kramer, Phys. Rev. Lett. **84**, 1934 (2000).
[5] see e.g. R. Neubecker and T. Tschudi, eds., spec. issue *Pattern Formation in Nonlinear Optical Systems*, Chaos, Solitons & Fractals **10** (4-5) (1999); F.T. Arecchi, S. Boccaletti and P.L. Ramazza, Physics Reports **318**, 1 (1999) and references therein.
[6] for a recent review paper on the LCLV see F.T. Arecchi, S. Boccaletti, S. Ducci, E. Pampaloni, P.L. Ramazza and S. Residori, J. of Nonlinear Opt. Phys. and Materials 9, 183 (2000).
[7] V. Fréedericksz and V. Zolina, Trans. Faraday Soc. **29**, 919 (1933).
[8] P. G. de Gennes and J. Prost, *The Physics of Liquid Crystals*, (Oxford Science Publications, Clarendon Press, second edition, 1993).

[9] S. Chandrasekhar, *Liquid Crystal*, (Cambridge, New York, 1992).
[10] M.G. Clerc, S. Residori and C.S. Riera, Phys. Rev. E **63**, 060701 (2001).
[11] S.A. AKhmanov, M.A. Vorontsov and V.Yu. Ivanov, JETP Lett. **47**, 707 (1988).
[12] L.D. Landau and E.M. Lifshitz, *Statistical physics* (Pergamon Press, New York 1969).
[13] W.K. Burton, N. Cabrera, and F.C. Frank, Phil. Trans. Roy. Soc. London A 243, 299 (1951).
[14] K. Kawasaki and Otha, Physica A **116**, 573 (1982).
[15] P. Coullet, L. Gil and D. Repaux, *Instabilities and Nonequilibrium Structures II*, edited by E. Tirapegui and D. Villaroel (Kluwer, Dordrecht, 1989).
[16] R.A. Fisher, Ann. Eugenics, **7**, 335 (1937).
[17] A. Kolmogorov, I. Petrovsky, and Piskunov, Bull. Univ. Moskou Ser. Int. Se. **7**(6), 1 (1937).
[18] D.G. Aronson and H.F. Weinberger, Adv. Math. **30** 33 (1978).
[19] M. Cross and P. Hohenberg, Rev. Modern Phys. **65**, 581 (1993).
[20] P.L. Ramazza, S. Residori, E. Pampaloni, A.V. Larichev, Phys. Rev. A **53**, 400 (1996).

(M.G. Clerc) Departamento de Física, Facultad de Ciencias Físicas y Matemáticas, Universidad de Chile, Casilla 487-3, Santiago, Chile.

(A. Petrossian) Physics Department, Yerevan St. University 1, A. Manoogian st. 375049 Yerevan, Armenia.

(S. Residori) Institut Non Linéaire de Nice, UMR 6618 CNRS-UNSA, 1361 Route des Lucioles, F-065600 Valbonne, France.

(C.S. Riera) DAMTP, Silver street, Cambridge CB3 9EW, U.K.